atmosphere

MDPI

Article

Application of the Self-Organizing Map Method in February Temperature and Precipitation Pattern over China: Comparison between 2021 and 2022

Zengping Zhang [1,2], Yu Gu [3,*], Zhikuan Wang [2], Siyuan Luo [4], Siyuan Sun [2], Shuting Wang [2] and Guolin Feng [2,5,*]

1 College of Mathematics Science and Technology, Yangzhou University, Yangzhou 225002, China
2 College of Physical Science and Technology, Yangzhou University, Yangzhou 225002, China
3 Jiangsu Yangzhou Meteorological Bureau, Yangzhou 225009, China
4 Beijing Meteorological Bureau, Beijing 102600, China
5 China Meteorological Administration, Beijing 100081, China
* Correspondence: 20171101044@nuist.edu.cn (Y.G.); fenggl@cma.gov.cn (G.F.)

Abstract: In this study, we compared two anomalous wet February periods in 2021 and 2022 in China. The same anomalies appeared in the spatial distribution of precipitation, with anomalous precipitation centered over the southeast coast. However, temperature discrepancies appeared in most of China, with anomalously high temperatures in 2021 and lower temperatures in 2022. Both instances of increased precipitation were attributed to warm and moist advection from the south, with transport in 2021 being partly enhanced by the South China Sea cyclone, whereas transport in 2022 was mainly due to the subtropical western North Pacific anticyclone. Therefore, in this study, we aimed to compare and analyze temperature and precipitation anomalies in February 2021 and 2022 using the self-organizing map method. Warm events in East Asia and cold events in Siberia and the Tibetan Plateau types were obtained by mode 1, which contained 2021. Mode 6 exhibited opposite warm types in Siberia and cold types in southern Asia, including February temperature and precipitation anomalies in 2022. Based on the results of this study, we can conclude that precipitation anomalies in February 2021 and 2022 occurred under different temperature and circulation anomalies, and both were influenced by La Niña events. Autumn sea ice loss in the Barents Sea contributed significantly to warm and rainy events in February 2021. However, the cold and rainy events of February 2022 were closely related to the strengthening of the Siberian High.

Keywords: self-organizing map; South China Sea cyclone; subtropical western North Pacific anticyclone; Siberian High

Citation: Zhang, Z.; Gu, Y.; Wang, Z.; Luo, S.; Sun, S.; Wang, S.; Feng, G. Application of the Self-Organizing Map Method in February Temperature and Precipitation Pattern over China: Comparison between 2021 and 2022. *Atmosphere* **2023**, *14*, 1182. https://doi.org/10.3390/atmos14071182

Academic Editor: Shanshan Wang

Received: 26 June 2023
Revised: 18 July 2023
Accepted: 19 July 2023
Published: 21 July 2023

1. Introduction

During the early winter of 2020/21, China suffered three striking cold events, two of which affected an area ranging from northern to southern China [1]. Low temperature records were broken in 58 cities. The temperatures were at least 1–2 °C below the normal range across the country. Moreover, the temperatures of some regions dropped 4 °C below what was normal [2]. The impressive cold events in China during the early winter of 2020/21 gained the attention of many researchers [3,4]. However, during the second half of the winter of 2020/21, mainly in February 2021, China experienced a homogeneous warm pattern. Meanwhile, most of China experienced anomalous rainy conditions. Other severe and noteworthy anomalous winter rainy conditions hit China in February 2022, with maximum precipitation centered in southeastern China. Extremely heavy precipitation of 178.16 mm that broke the 1980 record was observed in both the Guangdong and Guangxi provinces. Even worse, historical cold air masses struck southern China, especially in the Guangdong and Guangxi provinces, which had the fourth-lowest temperature records from 1961 to 2022. The average temperature during this time period was approximately 2.39 °C

below normal in most of China [https://cmdp.ncc-cma.net/cn/index.htm (accessed on 21 June 2023) (in Chinese)]. Such variability in winter precipitation and temperature over China is worthy of attention to facilitate risk mitigation.

Variations in winter precipitation and temperature over China have been topics of great concern. Large-scale atmospheric circulation anomalies directly influence extremely cold or rainy conditions in winter over most parts of China. Yuan and Li [5,6] found that the negative Arctic Oscillation (AO) co-occurred with the stronger Siberian High (SH), which led to cold air from the polar regions advecting southward, causing enhanced extreme cold days in winter. Meanwhile, the negative AO and stronger SH may be related to excessive snow over north-eastern Eurasia. The intensified Ural High and deepened East Asian Trough also guided strong cold air transport processes invading China, which induced extreme cold and precipitation events [1]. In addition, the eastward propagation of Rossby waves along the subtropical westerly jet over South Asia contributes to the occurrence of heavy winter precipitation or extreme cold events over China [7,8]. When the Asian jet shifts southward and intensifies, the trough over Europe and western Asia synchronously shifts southeastward, which enhances the Rossby wave train [9]. Li and Sun [6] reported that the extreme rainstorm that hit southern China in December 2013 was closely related to the Rossby waveguide within a subtropical westerly jet.

In addition to the impact of large-scale atmospheric circulation anomalies, the East Asian winter monsoon and El Niño-Southern Oscillation (ENSO) are widely regarded as the main factors of extreme winter temperature and precipitation events [10–12]. A strong East Asian winter monsoon is usually accompanied by below-normal precipitation over southeastern China [13]. Increased winter precipitation over southern China tends to occur when the East Asian winter monsoon weakens and El Niño events occur [14,15]. The strong southerly wind anomaly and enhanced anticyclonic circulation anomaly in the Western Pacific Region collectively result in more precipitation in China during El Niño events [16,17]. In contrast, the East Asian winter monsoon is strong, and La Niña after 1980 may lead to an enhanced and more northward subtropical westerly jet over East Asia in winter. Since southern China is rightly located on the right side of the jet entrance region, anomalous ascending motion dominates there through the secondary vertical circulation, favoring more winter precipitation in southern China [18,19]. La Niña events usually induce an anomalous lower-tropospheric cyclone over the western North Pacific, which favored the convergence of water vapor over central and southern China and led to freezing rain in January 2008 [20]. The 2020–2022 La Niña event started in August 2020 with a Niño-3.4 index exceeding −0.5 °C [1]. Meanwhile, in the first half of winter 2020/21, China experienced an extremely cold period, with many stations having record-breaking low temperatures. The large-scale atmospheric circulation anomalies in the Northern Hemisphere were influenced by the negative AO, strengthened SH, intensified Ural High, and deepened East Asian Trough [21,22]. Moreover, the synergistic effects of the warm Arctic and La Niña are regarded as related factors [23]). The precipitation in February 2022 over China reached the eighth since 1961, with precipitation 0.5 to 2 times higher than normal, which also occurred during La Niña events [24]. In addition, lower temperatures, freezing, and insufficient sunshine are detrimental to the growth of crops, the economy, and traffic.

Therefore, it is of great scientific interest to further analyze why extreme precipitation occurred in February 2021 and 2022 with the different spatial and intensity distributions of temperature. The remainder of this paper is organized as follows: Section 2 introduces the datasets and diagnostic methods used. Section 3 describes the characteristics of temperature and precipitation in February 2021 and 2022. The favorable atmospheric conditions and related impacts are compared in Section 4. The conclusions and discussion are presented in Section 5.

2. Data and Methods

2.1. Datasets

The observed daily air temperature and precipitation datasets for 1961–2022 were provided by the National Meteorological Information Center of the China Meteorological Administration. When the proportion of missing data from the stations exceeded 5%, they were excluded. In addition, the remaining missing data from the selected stations was replaced with the climatological normal. Finally, 2128 stations were employed, as shown in Figure 1. The climatological period was from February 1961 to February 2022, which was used in our research.

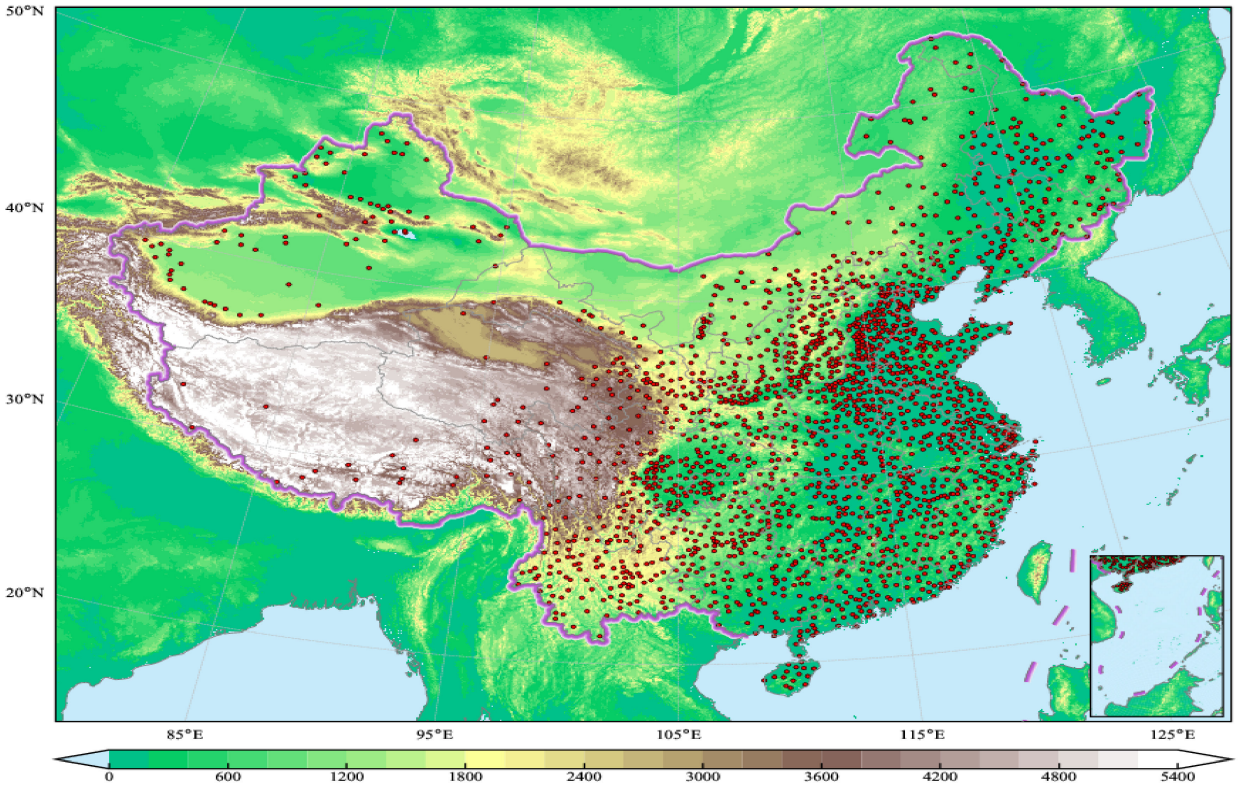

Figure 1. Topographic map of China (shading; Units: m) and location map of 2128 selected stations (red dots). The lower-right picture shows the South China Sea.

Atmospheric reanalysis of ERA5 was provided by the European Center for Medium-Range Weather Forecasts (ECMWF) from 1961 to 2022 [25]. The monthly 2-m air temperature (T2M), zonal and meridional wind, geopotential height, vertical velocity, and specific humidity were used with a spatial resolution of a 0.25° × 0.25° latitude/longitude grid [26]. In addition, global monthly average sea ice concentration (SIC) data from 1961 to 2022 were obtained from the Met Office Hadley Center with a grid resolution of 1° × 1° latitude/longitude [27,28]. Additionally, we calculated the average SIC in the Arctic for four months (August to November).

2.2. Methods

Self-organizing map (SOM) analysis is an unsupervised neural network method based on competitive learning that can nonlinearly map high-dimensional input samples to a set of two-dimensional grid points [29]. Based on the principle of the neural network, the method repeatedly learns and trains meteorological elements and obtains the dominant circulation mode [30]. In addition, the SOM patterns for the boreal winter resemble more closely the observed daily data than those obtained using the empirical orthogonal function [31]. Thus, SOM has been widely used to distinguish weather patterns in atmospheric circulation [32,33].

In this study, SOM training and analysis were based on monthly spatial anomalies of T2M in February of the years 1961–2022. After SOM training, additional input data can be mapped to the nodes by calculating the Euclidean distance [34]. Subsequently, the SOM for the February T2M was shown using rectangular lattices with 3 × 3 modes (Figure 2).

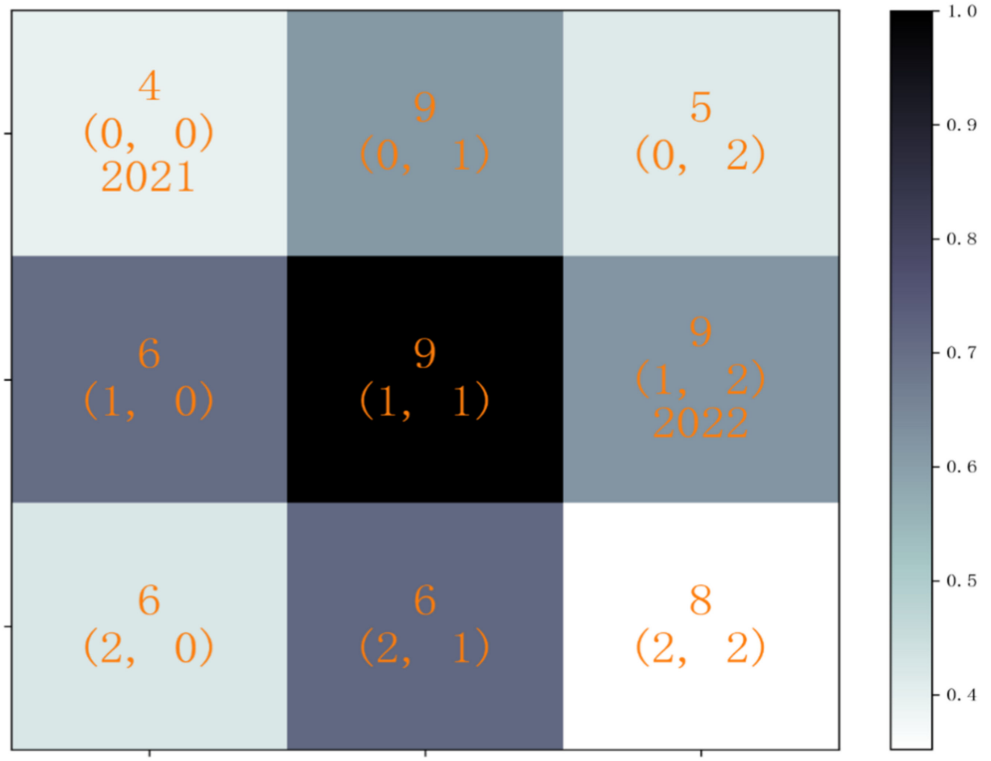

Figure 2. Diagram of the SOM training results. The numbers in brackets in the figure represent the number of each model after the classification, and the numbers above represent the sample size, where 2021 and 2022 are located in Model 1 and Model 6, respectively.

In addition, composite analyses of the circulation and sea ice anomalies were derived. A student's *t*-test was used to assess the statistical significance level shown in the figures, as the dots denote regions in the figures that exceeded the 95% confidence level and were marked as significant. The vertically integrated water vapor transport flux (WVT) was calculated from the surface to 100 hPa according to the method proposed by Trenberth [35]).

3. Variations in February Temperature and Precipitation in 2021 and 2022

In winter, temperature and precipitation are greatly reduced throughout China at lower latitudes [36]. In February 2021, anomalously high temperatures occurred in most of China, especially in the eastern regions (Figure 3a). However, during the first half of the winter of 2020/21, China suffered strong cold air processes, which were exactly the opposite of February [2]. Heavy precipitation in February occurred mainly over most of China, with the maximum occurring near the Yangtze River valley (Figure 3b), whereas the precipitation over northern China was close to normal. In February 2022, low temperatures were reported in southern China, northern China, and the eastern Tibetan Plateau, with cumulative daily mean temperature drops of approximately 4 °C in southern China based on the climatological period from 1961 to 2022 (Figure 3c). Accordingly, positive precipitation anomalies were observed throughout the region (Figure 3d). The precipitation at some stations over southern China had broken records. Extremely heavy precipitation of 178.16 mm was observed in both the Guangdong and Guangxi provinces and broke the 1980 record. Even worse, historical cold air masses struck southern China, especially in the Guangdong and Guangxi provinces. Extreme precipitation occurred in the Yangtze

River Valley and southern China in February 2021 and 2022, featuring diversity in their meridional displacement.

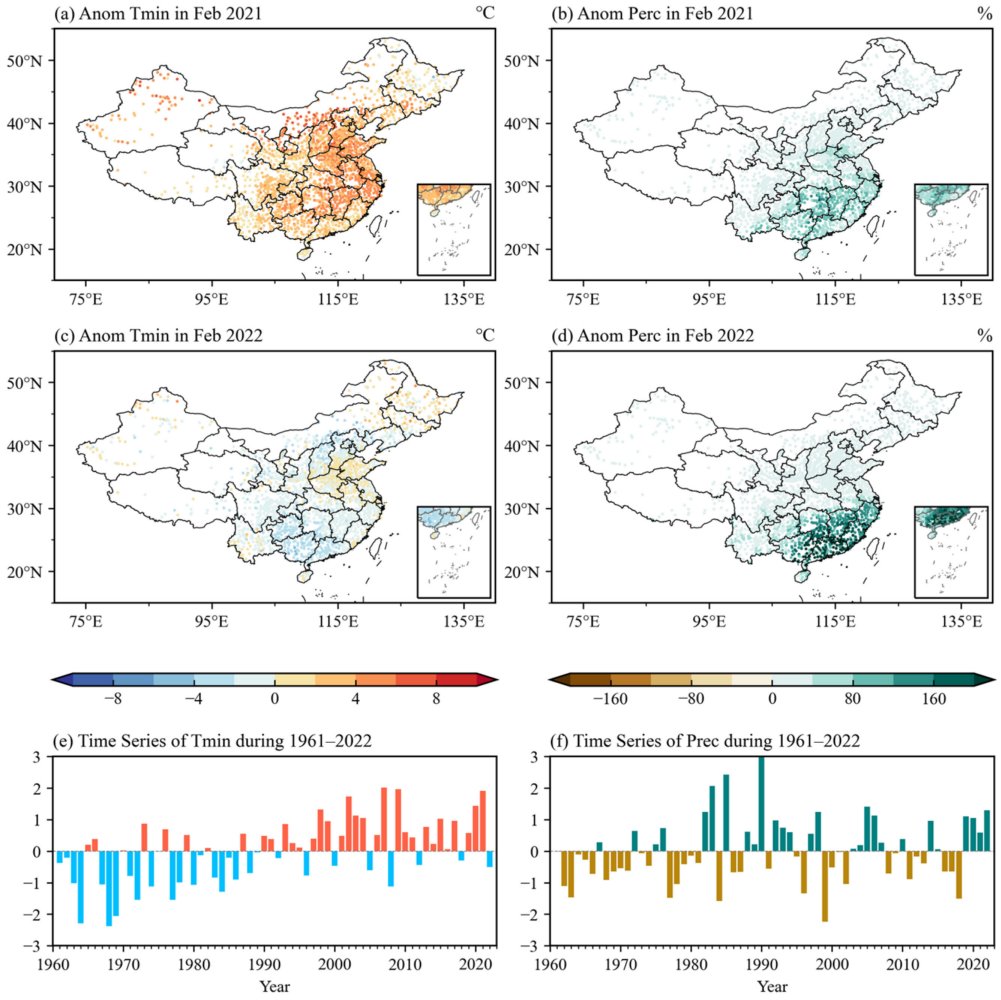

Figure 3. Temperature anomaly (scatter; Units: °C) and precipitation anomaly percentage (scatter; Units: %) over China in February of (**a**,**b**) 2021 and (**c**,**d**) 2022, respectively. Time series of anomalous temperature (**e**) and precipitation (**f**) over China in February from 1961 to 2022.

4. Atmospheric Conditions in February 2021 and 2022

4.1. Circulation Patterns in February 2021 and 2022

Atmospheric circulation anomalies can cause temperature and precipitation anomalies directly. In this section, we discuss the circulation characteristics associated with the February temperature and precipitation anomalies in 2021 and 2022. The zonal wind from 200 hPa over East Asia to the Western Pacific (10–150° E, 30–40° N) was weak in February 2021 (Figure 4a). The maximum jet centers were located near 120–150° E and 30–40° N. In the middle troposphere, anomalously high pressure predominantly controlled western and northern China. An anomalous cyclone was centered over Europe (Figure 4c). The East Asian trough was westward and weaker than usual, and it mainly reached close to the Yangtze River valley. At the same time, as shown in Figure 4e, strong moisture transportation and strong convergence over the South China Sea combined with the East Asian trough provided adequate dynamic and moisture conditions for precipitation, especially over the Yangtze River valley.

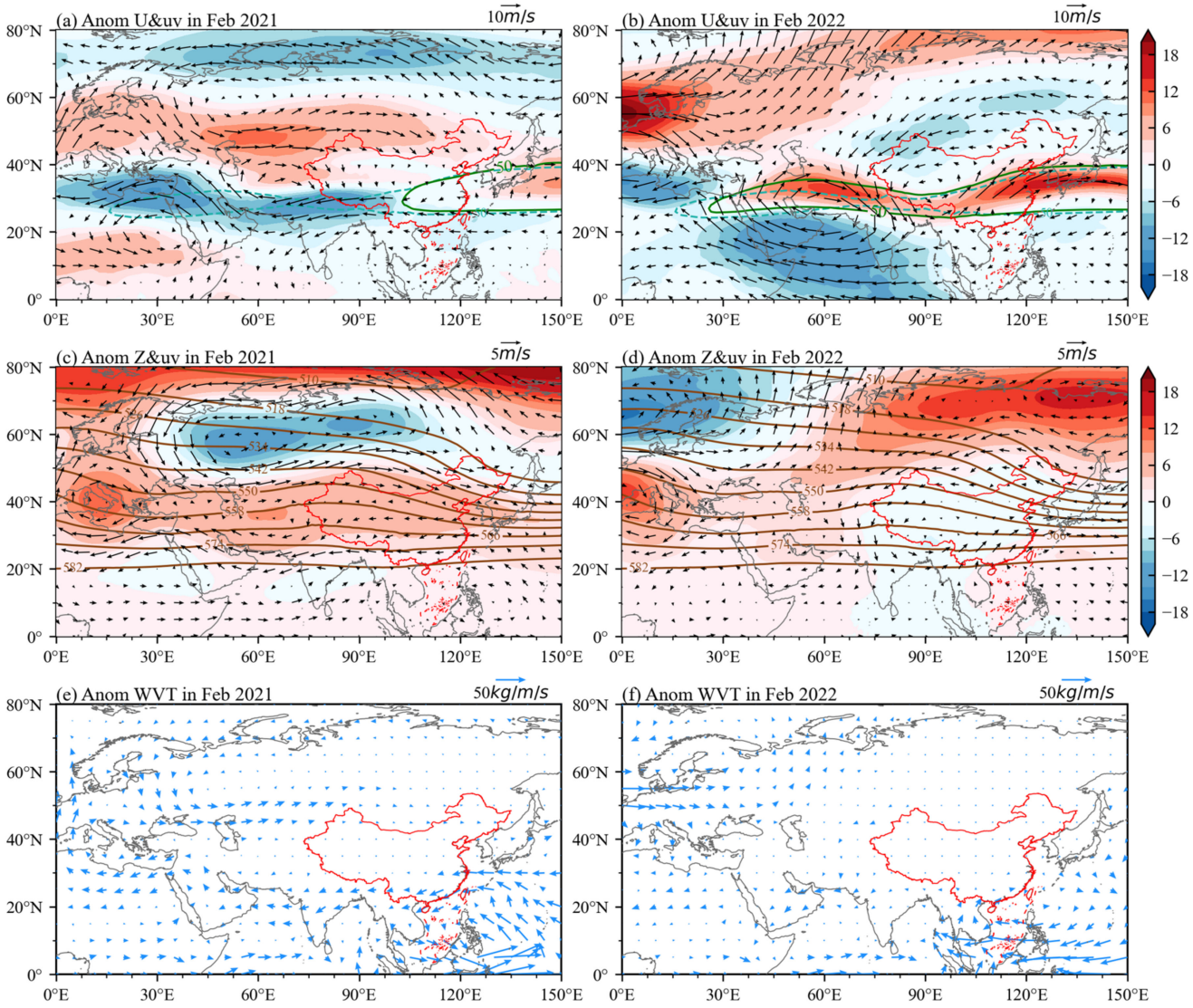

Figure 4. Characteristics of the anomalous atmospheric circulation in February: (**a**,**b**) 200 hPa zonal wind (shading, Units: m·s−1; the dashed and solid green lines represent the 30 m·s−1 isoline in the climatological mean) and wind field (vectors, Units: m s−1); (**c**,**d**) 500 hPa geopotential height (shading, Units: gpm; the solid brown lines are the climatological mean of geopotential height) and wind field (vectors, Units: m s−1); (**e**,**f**) WVT (vectors, Units: kg·m−1 s−1). The left column is for 2021, and the right column is for 2022, respectively.

In contrast, as shown in Figure 4b, the zonal wind from 200 hPa over East Asia to the Western Pacific (30–180° E, 30–40° N) was strong in February 2022. The maximum jet centers were located near 50–80° E, 30° N, and 110–150° E, 30–40° N. Southern China is located south of the jet-stream axis. The geopotential height at 500 hPa showed that most of China was dominated by anomalously low pressure, which caused the deepened East Asian trough (Figure 4d). Meanwhile, the Siberian High was strong, which led to more cold airflow invading China and causing extreme cold events. In addition, the west-extending subtropical high over the western Pacific Ocean to southeastern China provided abundant water vapor conditions for the anomalous February precipitation in 2022 (Figure 4f).

It is inferred that although February 2021 and 2022 correspond to La Niña events, anomalous precipitation is accompanied by different temperatures and contemporaneous anomaly patterns in the troposphere (Figure 4). It is interesting to note that these anomalous atmospheric circulations favor enhanced temperature and precipitation anomalies.

4.2. The SOM Modes

SOM is regarded as a very effective tool for distinguishing different weather patterns. Thus, in this study, we applied SOM to classify the February T2M anomalies from 1961 to 2022 [22]. For the spatial distribution of temperature in February, the best matching unit (BMU) was obtained by calculating the Euclidean distance between T2M and the nine SOM modes shown in Figure 2. Figure 5 shows the time series of the BMU in February from 1961 to 2022 for T2M, in which types 1 and 6 contained similar temperature distribution characteristics to 2021 and 2022, respectively.

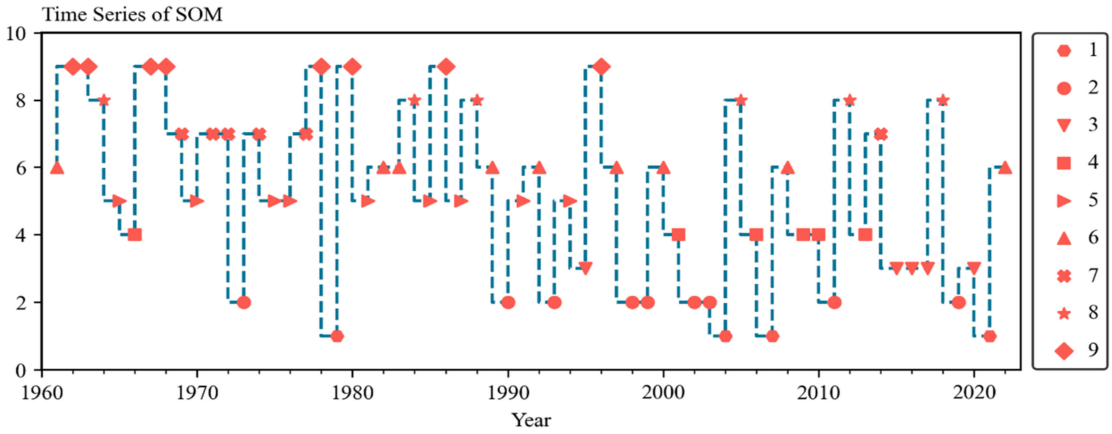

Figure 5. Temporal evolution of the BMU for the nine (3 × 3) SOM modes.

Warm events in East Asia and cold events in Siberia and the Tibetan Plateau were obtained by type 1 (Figure 6a) and represented by a hexagon. Types 2 and 3 were warm in Eurasia, and type 3 was warm in western Siberia (Figure 6b,c), represented by circles and inverted triangles. Warm events in eastern Asia and cold events in eastern Siberia and in the Arctic Ocean north of western Siberia are shown in Figure 5d,e, and types 4 and 5 are represented by rectangles and right triangles, respectively. Type 6 is represented by a triangle with opposite warm and cold types in Siberia and South Asia (Figure 6f). Type 7 was mostly cold in Eurasia and insignificantly warm in the Tibetan Plateau (Figure 5g), represented by × symbols, while types 8 and 9 were more frequent cold in eastern Asia and significantly warm in the Arctic Ocean north of western Siberia and Siberia, and are represented by star and diamond symbols, respectively (Figure 6h,i). Interannual changes in T2M in different regions are shown in Figure 3.

Based on the classification of T2M by the SOM method, we synthesize the precipitation anomalies in eastern China, as shown in Figure 7 in each model. As can be seen from the synthesis of February precipitation in different SOM modes, precipitation mode 1 was mainly located in the Yellow River Basin, Sichuan Basin, and Yunnan-Guizhou Plateau, which contained February precipitation in 2021 (Figure 7a). Modes 2 and 5 were the rainfall patterns centered in eastern China, especially north of the Yangtze River (Figure 7b,e). In mode 3, precipitation was concentrated in the Sichuan Basin (Figure 7c). The precipitation patterns in modes 4, 7, and 8 were mainly located in the northern Yangtze River (Figure 7d,g,h). However, in mode 6, when the northern Yangtze River experienced drought, the precipitation in southern China was higher, and the precipitation anomaly was more significant (Figure 7f). Mode 6 included February precipitation in 2022. Mode 9 reflected the opposite change, with drought occurring in most regions, especially in the middle and lower reaches of the Yangtze River (Figure 7i). Although the T2M SOM pattern corresponds well with precipitation, the physical processes that cause temperature and precipitation are complex. Therefore, it is necessary to further analyze the configuration of the circulation system in each mode.

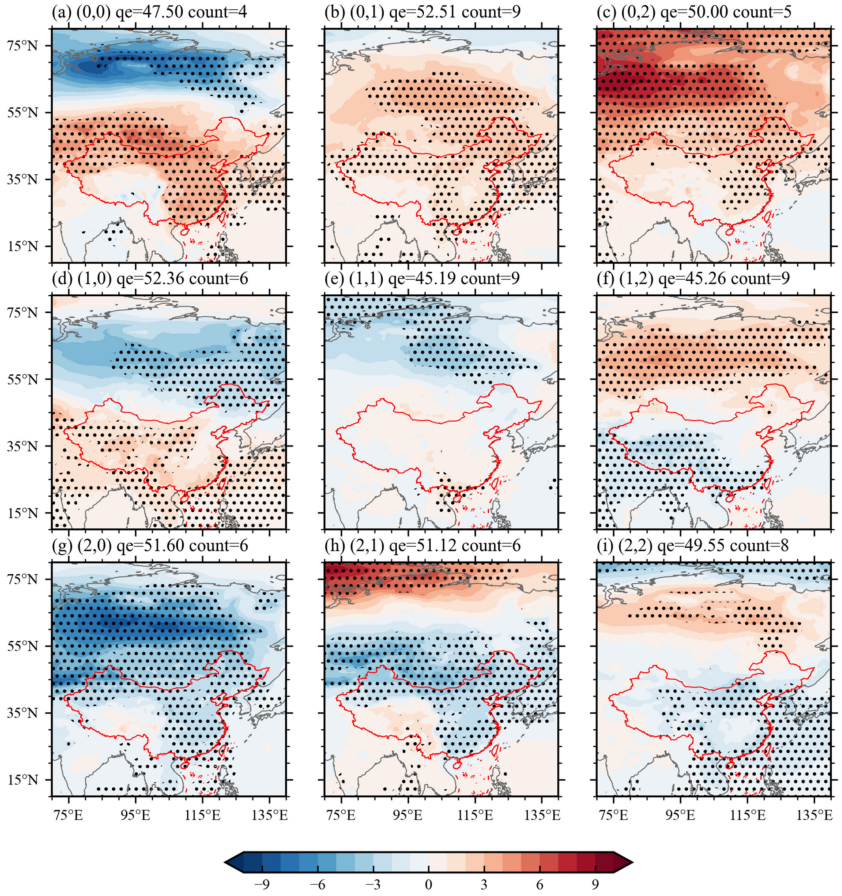

Figure 6. Nine (3 × 3) SOM modes of the February T2M anomaly (Units: °C) from 1961 to 2022. The dots denote regions in which the differences exceed the 95% confidence level, which is based on the student's *t*-tests.

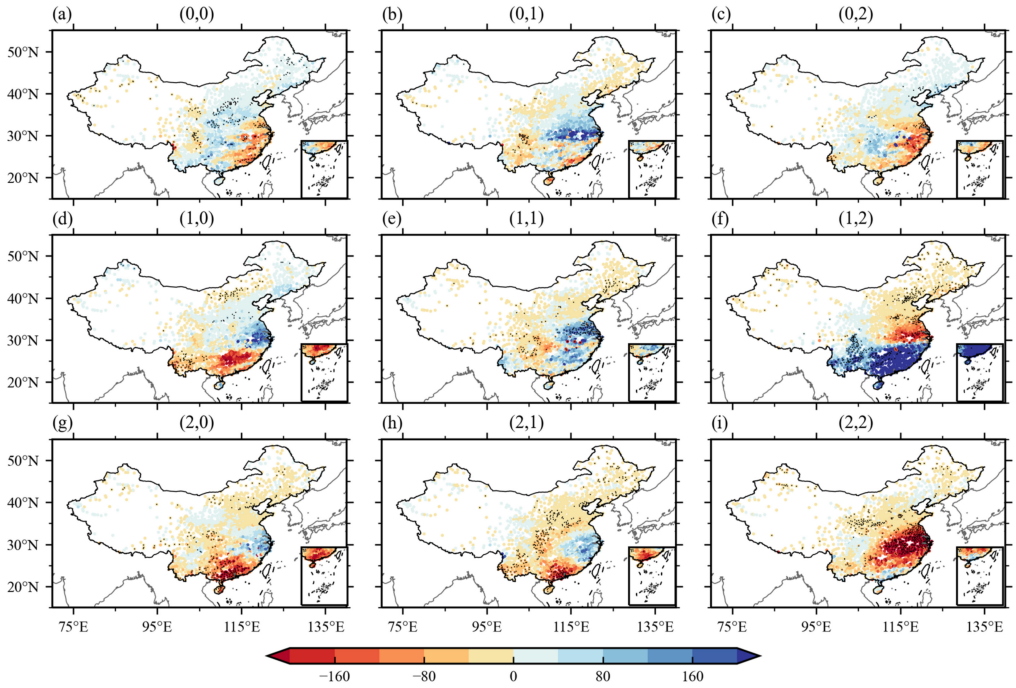

Figure 7. Composites of the precipitation anomaly percentage (Units: %) of the SOM patterns. The dots denote regions in which the differences exceed the 95% confidence level.

4.3. Association between SOM Modes and Large-Scale Circulation

We synthesized geopotential heights at 500 hPa and wind fields at 200 hPa based on the corresponding year of SOM classification shown in Figure 5. A comparison of Figures 6 and 7 with Figure 8 revealed a close association between the spatial characteristics of the anomalous February temperature and precipitation and the circulation patterns. In conjunction with mode 1, there were significant negative geopotential height anomalies centering over Mongolia and northeastern China and significantly positive geopotential height anomalies over the northwestern Pacific Ocean, which were consistent with the temperature anomalies (Figure 8a). The enhanced low pressure likely deepened the East Asian trough and led to precipitation anomalies. Meanwhile, the position of the hypoactive westerly jet caused more precipitation in the south of the Yangtze River, which was very similar to the temperature and precipitation anomalies in February 2021. As shown in Figure 8b, the positive height in mainland China weakened, while the negative height strengthened, and the westerly jet was strong. The anticyclone in the north of the Bay of Bengal and the strengthened cyclone over Mongolia led to warm and cold air converging in the north Yangtze River, which increased precipitation. The third mode exhibited a low-pressure center located in northwest China (Figure 8c) and had higher temperatures and lower precipitation. When a significant cyclone anomaly occurred over West Siberia, the East Asian trough was likely to increase the precipitation in the Yangtze River (Figure 8d). In mode 5, the anomalous centers were not significant, and the positive height in mainland China, especially in eastern China, was similar to mode 1 but affected more precipitation along the southeast coast regions (Figure 8e). The extreme precipitation in 2022 was related to the enhanced Siberian High, northwest Pacific, and Indian Peninsula cyclones (Figure 8f). Sufficient warm moisture and strong cold air converged over southern China, thereby promoting temperature and precipitation anomalies. Modes 7 and 8 showed similar circulation anomalies to anticyclones over mainland China and cyclones over northwest Europe. Meanwhile, the westerly jet weakened (Figure 8g,h). Thus, most of China experienced a cold anomaly, and the precipitation was mainly centered in the eastern coastal regions. Finally, uniform cold and drought anomalies across the region were affected by the enhanced cyclone over the Tibetan Plateau. The East Asian trough was induced by the anticyclone over Mongolia, which was accompanied by an enhanced westerly jet and prevailing westerlies.

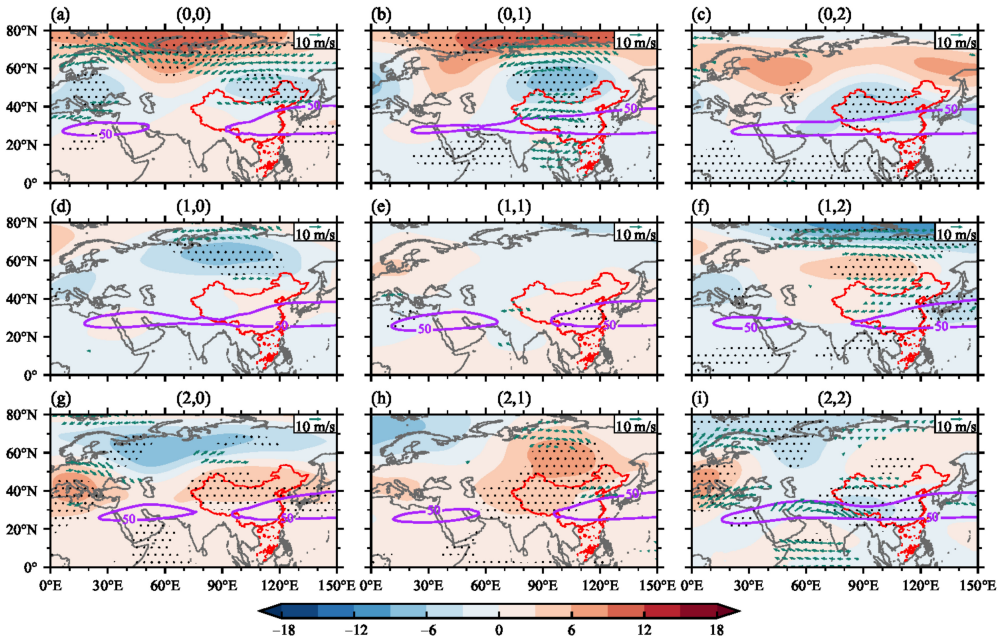

Figure 8. Circulation configuration of nine SOM patterns in a 500 hPa geopotential height (shading, Units: gpm), 200 hPa wind field (vectors, Units: m s−1) and 50 m·s−1 zonal wind isoline (purple lines, Units: m s−1). The dots denote regions, and green vectors mean they exceed the 95% confidence level.

5. Conclusions and Discussion

Winter precipitation is accompanied by lower temperatures, which usually generate serious freezing disasters and have a significant impact on traffic, agriculture, the economy, and humans. Commonly, La Niña events play a crucial role in winter precipitation over China; however, the extreme rainfall in February 2021 and 2022 was beyond prediction [24]. The results of this study can provide a reference for further study of the mechanisms underlying the causes of winter precipitation in China.

Severe cold air broke out in most of China in early winter (from December 2020 to January 2021; [2]). However, during February 2021, most of China experienced a positive temperature anomaly and unusual precipitation, particularly in the Yangtze River. Furthermore, in February 2022, more severe precipitation and snow broke the historical record, particularly in southern China, during which cold air prevailed in southern and northern China. Therefore, in this study, we aimed to compare and analyze temperature and precipitation anomalies in February 2021 and 2022 using the SOM method. February T2M was classified into 3 × 3 SOM modes. Warm in East Asia and cold in Siberia and the Tibetan Plateau types were obtained by mode 1, which contained 2021. Mode 6 exhibited opposite warm and cold types in Siberia and southern Asia and included February temperature and precipitation anomalies in 2022. The diagnostic analysis revealed that warm and rainy events in February 2021 were coherently linked to (a) the strengthening of the Mongolian low pressure, (b) the strengthening of the Western Pacific Subtropical High, and (c) the weakening westerly jet. However, the cold and rainy events in February 2022 were coherently linked to (a) the strengthening of the Siberian High, (b) the weakening Western Pacific Subtropical High, and (c) the westerly jet. In addition, many previous studies have shown that the area extent, concentration, and thickness of sea ice in the Arctic Ocean and adjacent seas have strongly decreased during the past few decades [2]. Especially the sea ice around the Barents Sea [37]. The reduction of sea ice in the Barents Sea can have implications for circulation systems across Eurasia. Firstly, the decrease in sea ice directly impacts heat flux over the polar oceans, albedo in the Barents region, and the thermal gradient from mid-latitudes to polar regions. This triggers quasi-stationary Rossby waves in the mid-to-high-latitude regions of Eurasia, leading to the emergence of the Euro-Asian (EU) teleconnection pattern [38]. Furthermore, in terms of thermodynamic processes, it can influence remote teleconnection patterns in the mid-to-high-latitude regions of Eurasia by altering the distribution of spring snow cover and associated soil moisture anomalies [24,39]. Consequently, these changes affect the circulation system of East Asia as a whole, resulting in anomalous circulation patterns that impact the local weather system in China. Wang et al. [22] emphasized that sea ice loss significantly contributed to the 2020/2021 winter circulation and temperature anomalies. SIC loss varied in autumn 2020 and 2021 (Figure 9). Thus, the unusual autumn Arctic warming and substantial sea ice loss in 2020/2021 may have contributed to this temperature and precipitation. In autumn 2020, Arctic Sea ice loss, especially in the Barents Sea, decreased significantly. The circulation anomalies were consistent with a significant decline in sea ice. As for sea ice loss in autumn 2021, the Arctic Sea ice reduction was insignificant (Figure 9). Thus, we can conclude that the February precipitation anomalies in 2021 and 2022 occurred under different temperature and circulation anomalies, and both were influenced by La Niña events. Autumn sea ice loss in the Barents Sea significantly contributed to warm and rainy events in February 2021. However, the cold and rainy events in February 2022 were closely related to the strengthening of the Siberian High.

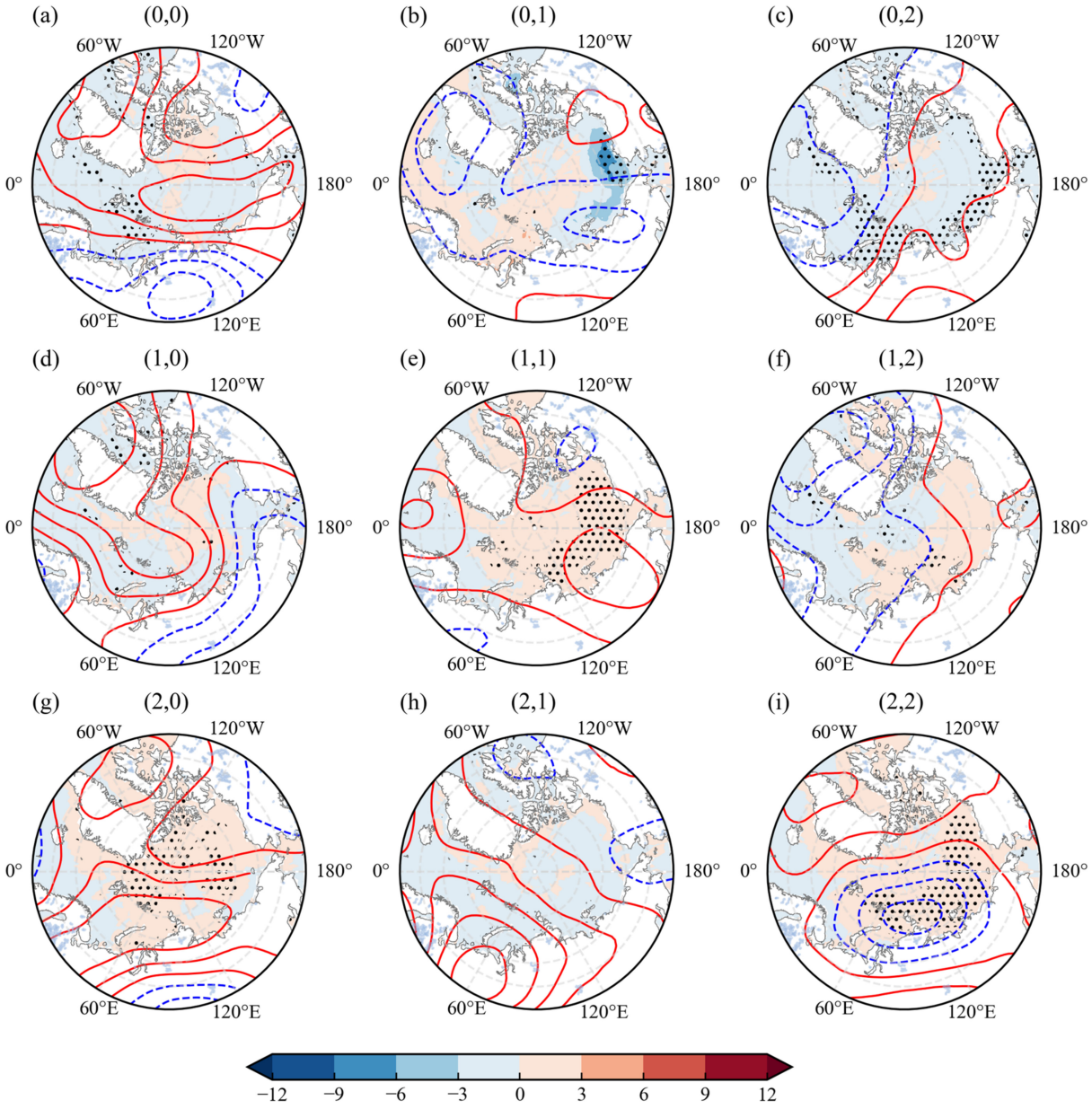

Figure 9. Spring SIC (shading, Units: %) and 500 hPa geopotential height (contours, Units: gpm) anomalies of nine SOM. The dots denote regions in which the differences exceed the 95% confidence level. The solid red line represents the positive value of the 500 hPa geopotential height, the blue dashed line represents the positive value of the 500 hPa geopotential height.

Notably, three consecutive years of La Niña events led to a more complex winter precipitation mechanism in China. During February 2021 and 2022, the precipitation situation was different from that of La Niña events in previous studies [19,21]). Specific factors, such as the tropical Atlantic, which were associated with atmospheric responses during the La Niña winter of 2021/2022, require further research [24]. In addition, previous studies have found that snow cover changes over the Tibetan Plateau may have impacts on interannual variations in winter precipitation over China [40]. Previous studies have also shown that snow cover changes over the Tibetan Plateau exhibit salient influences on the East Asian monsoon [41,42]. However, the changes in sea surface temperature associated with La Niña events might influence the westerly flows and collaborate with the dynamic and thermal effects of the Tibetan Plateau, which may also change the large-scale circulation patterns and influence winter precipitation over China [43,44]. The reason

that the temperature and precipitation situations in the winters of 2021 and 2022 were different from those of La Niña in the years examined in previous studies also needs to be studied further. SOM can help identify and detect patterns and characteristics of extreme events. By training on historical data, SOM can identify outliers and anomalous patterns, allowing potential extreme events to be detected in advance. This has a profound impact and research significance on the prediction of extreme events, which also needs to be studied further.

Author Contributions: Methodology, Y.G., Z.W., S.L.; software, Z.Z.; formal analysis, Y.G.; writing—original draft preparation, S.S.; resources, S.W.; funding acquisition, G.F. All authors have read and agreed to the published version of the manuscript.

Funding: This research is supported by the National Natural Science Foundation of China (grants No. 42175071 and No. 42130610), and Natural Science Foundation of Tibet Autonomous Region (grant NO. XZ202101ZR0041G).

Institutional Review Board Statement: Not applicable.

Informed Consent Statement: Not applicable.

Data Availability Statement: Precipitation data used during this study are openly available from the China Meteorological Administration at http://data.cma.cn/en (accessed on 21 June 2023). The Atmospheric reanalysis of ERA5 provided by the European Center for Medium-Range Weather Forecasts (ECMWF) can be accessed at: https://cds.climate.copernicus.eu/cdsapp#!/search?type=dataset (accessed on 21 June 2023), and the monthly average sea ice concentration obtained from the Met Office Hadley Center is available at: https://www.metoffice.gov.uk/hadobs/hadsst3/data/download.html (accessed on 21 June 2023).

Acknowledgments: The station-observed dataset is provided by the National Meteorological Information Center (NMIC), China.

Conflicts of Interest: The authors declare no conflict of interest.

References

1. Zheng, F.; Liu, J.P.; Fang, X.H.; Song, M.R.; Yang, C.Y.; Yuan, Y.; Li, K.X.; Wang, J.; Zhu, J. The predictability of ocean environments that contributed to the 2020/21 extreme cold events in China: 2020/21 La Niña and 2020 Arctic sea ice loss. *Adv. Atmos. Sci.* **2022**, *39*, 658–672. [CrossRef]
2. Zheng, F.; Yuan, Y.; Ding, Y.; Li, K.; Fang, X.; Zhao, Y.; Sun, Y.; Zhu, J.; Ke, Z.; Wang, J.; et al. The 2020/21 extremely cold winter in China influenced by the synergistic effect of La Niña and warm Arctic. *Adv. Atmos. Sci.* **2022**, *39*, 546–552. [CrossRef]
3. Bueh, C.; Peng, J.; Lin, D.; Chen, B. On the two successive supercold waves straddling the end of 2020 and the beginning of 2021. *Adv. Atmos. Sci.* **2022**, *39*, 591–608. [CrossRef]
4. Yao, Y.; Zhang, W.; Luo, D.; Zhong, L.; Pei, L. Seasonal cumulative effect of Ural blocking episodes on the frequent cold events in China during the early winter of 2020/21. *Adv. Atmos. Sci.* **2022**, *39*, 609–624. [CrossRef]
5. Yuan, C.; Li, W. Variations in the frequency of winter extreme cold days in northern China and possible causalities. *J. Clim.* **2019**, *32*, 8127–8141. [CrossRef]
6. Li, X.; Sun, J.; Zhang, M.; Zhang, Y.; Ma, J. Possible connection between declining Barents Sea ice and interdecadal increasing northeast China precipitation in May. *Int. J. Climatol.* **2021**, *41*, 6270–6282. [CrossRef]
7. Ding, F.; Li, C. Subtropical westerly jet waveguide and winter persistent heavy rainfall in south China. *J. Geophys. Res. Atmos.* **2017**, *122*, 7385–7400. [CrossRef]
8. Li, X.; Wen, Z.; Huang, W.R. Modulation of South Asian Jet wave train on the extreme winter precipitation over Southeast China: Comparison between 2015/16 and 2018/19. *J. Clim.* **2020**, *33*, 4065–4081. [CrossRef]
9. Hu, K.; Huang, G.; Wu, R.; Wang, L. Structure and dynamics of a wave train along the wintertime Asian jet and its impact on East Asian climate. *Clim. Dyn.* **2018**, *51*, 4123–4137. [CrossRef]
10. Ding, Y. A statistical study of winter monsoons in East Asia. *J. Trop. Meteorol.* **1990**, *6*, 119–128.
11. Zhai, P.; Yu, R.; Guo, Y.; Li, Q.; Ren, X.; Wang, Y.; Xu, W.; Liu, Y.; Ding, Y. The strong El Niño of 2015/16 and its dominant impacts on global and China's climate. *J. Meteorol. Res.* **2016**, *30*, 283–297. [CrossRef]
12. Zhou, L.; Wu, R. Respective impacts of the East Asian winter monsoon and ENSO on winter rainfall in China. *J. Geophys. Res. Atmos.* **2010**, *115*, D2. [CrossRef]
13. Zhou, L.T. Impact of East Asian winter monsoon on rainfall over southeastern China and its dynamical process. *Int. J. Climatol.* **2011**, *31*, 677–686. [CrossRef]

14. Kim, J.-W.; Yeh, S.-W.; Chang, E.-C. Combined effect of El Niño-Southern Oscillation and Pacific decadal oscillation on the East Asian winter monsoon. *Clim. Dyn.* **2014**, *42*, 957–971. [CrossRef]
15. Ma, T.; Chen, W.; Feng, J.; Wu, R. Modulation effects of the East Asian winter monsoon on El Niño-related rainfall anomalies in southeastern China. *Sci. Rep.* **2018**, *8*, 1–9. [CrossRef]
16. Gao, T.; Zhang, Q.; Luo, M. Intensifying effects of El Niño events on winter precipitation extremes in southeastern China. *Clim. Dyn.* **2020**, *54*, 631–648. [CrossRef]
17. Zhang, R.; Sumi, A.; Kimoto, M. A diagnostic study of the impact of El Niño on the precipitation in China. *Adv. Atmos. Sci.* **1999**, *16*, 229–241. [CrossRef]
18. Gao, H.; Yang, S. A severe drought event in northern China in winter 2008–2009 and the possible influences of La Niña and Tibetan Plateau. *J. Geophys. Res. Atmos.* **2009**, *114*, D24. [CrossRef]
19. Yuan, Y.U.A.N.; Li, C.; Yang, S. Decadal anomalies of winter precipitation over southern China in association with El Niño and La Niña. *J. Meteorol. Res.* **2014**, *28*, 91–110. [CrossRef]
20. Wen, M.; Yang, S.; Kumar, A.; Zhang, P. An analysis of the large-scale climate anomalies associated with the snowstorms affecting China in January 2008. *Mon. Weather Rev.* **2009**, *137*, 1111–1131. [CrossRef]
21. Cheung, H.N.; Zhou, W.; Mok, H.Y.; Wu, M.C. Relationship between Ural–Siberian blocking and the East Asian winter monsoon in relation to the Arctic Oscillation and the El Niño–Southern Oscillation. *J. Clim.* **2012**, *25*, 4242–4257. [CrossRef]
22. Wang, S.; Liu, J.; Cheng, X.; Kerzenmacher, T.; Li, H.; Lu, R.; Hu, Y.; Chen, Z.; Braesicke, P. Has substantial sea ice loss along the Siberian coast contributed to the 2020/2021 winter cold wave in China? *Int. J. Climatol.* **2022**, *42*, 1–14. [CrossRef]
23. Wang, C.; Yao, Y.; Wang, H.; Sun, X.; Zheng, J. The 2020 summer floods and 2020/21 winter extreme cold surges in China and the 2020 typhoon season in the Western North Pacific. *Adv. Atmos. Sci.* **2021**, *38*, 896–904. [CrossRef] [PubMed]
24. Tang, Q.; Zhang, X.; Francis, J. Extreme summer weather in northern mid-latitudes linked to a vanishing cryosphere. *Nat. Clim. Change* **2014**, *4*, 45–50. [CrossRef]
25. Hoffmann, L.; Günther, G.; Li, D.; Stein, O.; Wu, X.; Griessbach, S.; Heng, Y.; Konopka, P.; Müller, R.; Vogel, B.; et al. From ERA-Interim to ERA5: The considerable impact of ECMWF's next-generation reanalysis on Lagrangian transport simulations. *Atmos. Chem. Phys.* **2019**, *19*, 3097–3124. [CrossRef]
26. Hersbach, H.; Bell, B.; Berrisford, P.; Hirahara, S.; Horányi, A.; Muñoz-Sabater, J.; Nicolas, J.; Peubey, C.; Radu, R.; Schepers, D.; et al. The ERA5 global reanalysis. *Q. J. R. Meteorol. Soc.* **2020**, *146*, 1999–2049. [CrossRef]
27. Feng, J.; Zhang, Y.; Ke, C. Relationship between Winter Precipitation in Barents–Kara Seas and September–October Eastern Siberian Sea Ice Anomalies. *Appl. Sci.* **2019**, *9*, 1091. [CrossRef]
28. Lim, E.P.; Hudson, D.; Wheeler, M.C.; Marshall, A.G.; King, A.; Zhu, H.; Hendon, H.H.; de Burgh-Day, C.; Trewin, B.; Griffiths, M.; et al. Why Australia was not wet during spring 2020 despite La Niña. *Sci. Rep.* **2021**, *11*, 1–15. [CrossRef]
29. Kohonen, T. Self-organized formation of topologically correct feature maps. *Biol. Cybern.* **1982**, *43*, 59–69. [CrossRef]
30. Johnson, N.C.; Feldstein, S.B.; Tremblay, B. The continuum of Northern Hemisphere teleconnection patterns and a description of the NAO shift with the use of self-organizing maps. *J. Clim.* **2008**, *21*, 6354–6371. [CrossRef]
31. Yuan, J.; Tan, B.; Feldstein, S.B.; Lee, S. Wintertime North Pacific teleconnection patterns: Seasonal and interannual variability. *J. Clim.* **2015**, *28*, 8247–8263. [CrossRef]
32. Lee, M.H.; Lee, S.; Song, H.J.; Ho, C.H. The recent increase in the occurrence of a boreal summer teleconnection and its relationship with temperature extremes. *J. Clim.* **2017**, *30*, 7493–7504. [CrossRef]
33. Yu, L.; Zhong, S.; Sun, B. Trends in the occurrence of pan-Arctic warm extremes in the past four decades. *Int. J. Climatol.* **2021**, *41*, 4460–4477. [CrossRef]
34. Johnson, N.C.; Feldstein, S.B. The continuum of North Pacific sea level pressure patterns: Intraseasonal, interannual, and interdecadal variability. *J. Clim.* **2010**, *23*, 851–867. [CrossRef]
35. Trenberth, K.E. Climate diagnostics from global analyses: Conservation of mass in ECMWF analyses. *J. Clim.* **1991**, *4*, 707–722. [CrossRef]
36. Li, C.; Sun, J. Role of the Subtropical Westerly Jet Waveguide in a Southern China Heavy Rainstorm in December 2013. *Adv. Atmos. Sci.* **2015**, *32*, 601–612. [CrossRef]
37. Lind, S.; Ingvaldsen, R.B.; Furevik, T. Arctic warming hotspot in the northern Barents Sea linked to declining sea-ice import. *Nat. Clim. Change* **2018**, *8*, 634–639. [CrossRef]
38. Budikova, D.; Ford, T.W.; Ballinger, T.J. United States heat wave frequency and Arctic Ocean marginal sea ice variability. *J. Geophys. Res. Atmos.* **2019**, *124*, 6247–6264. [CrossRef]
39. Zhang, R.; Sun, C.; LI, W. Relationship between the interannual variations of Arctic sea ice and summer Eurasian teleconnection and associated influence on summer precipitation over China. *Chin. J. Geophys.* **2018**, *61*, 91–105. [CrossRef]
40. Berghuijs, W.R.; Hrachowitz Woods, M. A precipitation shift from snow towards rain leads to a decrease in streamflow. *Nat. Clim. Change* **2014**, *4*, 583–586. [CrossRef]
41. Sun, H.; Liu, X. Impacts of dynamic and thermal forcing by the Tibetan Plateau on the precipitation distribution in the Asian arid and monsoon regions. *Clim. Dyn.* **2021**, *56*, 2339–2358. [CrossRef]
42. Su, B.; Xiao, C.; Zhao, H.; Huang, Y.; Dou, T.; Wang, X.; Chen, D. Estimated changes in different forms of precipitation (snow, sleet, and rain) across China:1961–2016. *Atmos. Res.* **2022**, *270*, 106078. [CrossRef]

43. Hanzhe, L.M. The Role of Warm North Atlantic SST in the Formation of Positive Height Anomalies over the Ural Mountains during January 2008. *Adv. Atmos. Sci.* **2011**, *28*, 246–256.
44. Geng, X.; Zhang, W.; Xiang, Y.; Jiang, F. Dominant spatiotemporal variability of wintertime precipitation days in China and the linkage with large-scale climate drivers. *Int. J. Climatol.* **2021**, *41*, 3561–3577. [CrossRef]